Science of the Total Environment 809 (2022) 151173

Contents lists available at ScienceDirect

Science of the Total Environment

journal homepage: www.elsevier.com/locate/scitotenv

Role of mesoscale eddies in the sustenance of high biological productivity in North Eastern Arabian Sea during the winter-spring transition period

Smitha B.R. [a,1,*], V.N. Sanjeevan [b], K.B. Padmakumar [c], Midhun Shah Hussain [c], T.C. Salini [d], J.K. Lix [d]

[a] Centre for Marine Living Resources and Ecology, Kochi, Kerala, India
[b] Kerala University of Fisheries and Ocean Studies, Kochi, Kerala, India
[c] Department of Marine Biology, Microbiology and Biochemistry, School of Marine Sciences, Cochin University of Science and Technology, Kochi, Kerala, India
[d] Department of Physical Oceanography, School of Marine Sciences, Cochin University of Science and Technology, Kochi, Kerala, India

HIGHLIGHTS

- Winter and early spring NEAS experiences enhanced primary production triggered by vertical mixing.
- Pockets of peak primary production in the NEAS are associated with mesoscale processes/eddies.
- The NEAS experience species succession during winter/spring from diatom - mixed diatom/*Noctiluca* - *Noctiluca*.
- Intensification in bloom and altered production pattern in the NEAS due to warming/stratification during winter-spring.

GRAPHICAL ABSTRACT

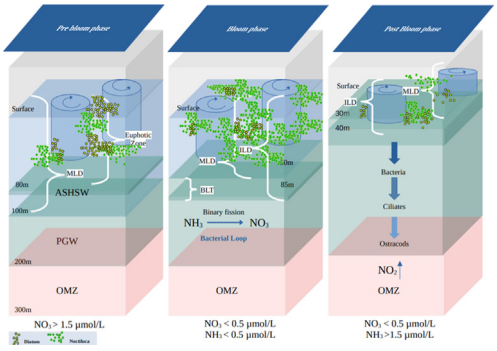

ARTICLE INFO

Article history:
Received 20 December 2020
Received in revised form 9 October 2021
Accepted 19 October 2021
Available online 24 October 2021

Editor: Julian Blasco

Keywords:
Cold core eddy
North Eastern Arabian Sea
Mesoscale process
Instability
Available Potential Energy
Algal bloom

ABSTRACT

Convective mixing, mesoscale eddies and regenerated production sustain an above-average biological productivity in the North East Arabian Sea (NEAS) during the winter-spring transition period. Satellite-derived long-term data sets on Chlorophyll-*a* (Chl-*a*), Sea Surface Height Anomaly (SSHA), Sea Surface Temperature (SST) and Okubo-Weiss parameterization show existence of number of mesoscale eddies, propagating and non-propagating, that contribute to the regional production. The dominance of Eddy Kinetic Energy (EKE) over the Available Potential Energy (APE) in the core depth and the diameter (120km) of the observed eddy being wider than the Rossby Radius of Deformation (RRD, 55 km), it is suggested that the baroclinic instability is a possible mechanism for the eddy formation. Spatial variation in APE and its influences on the regional dynamics, including chemical and biological response are explained. In the non-eddy areas, where convective mixing is active, diatoms (96.74%) dominated than dinoflagellates (3.14%), and the Chl-*a* in the Cold Core Eddy (CCE) were two to three folds higher to non-eddy regions. The abundance increased from core (58,152 cells L^{-1}) to periphery (5.95×10^5 cells L^{-1}) where the water column is less dynamic. Extensive blooms of the dinoflagellate green *Noctiluca* (*N. scintillans*) contribute to the very high cell density in the periphery of the CCE, where the currents were comparatively weak, and water column was more stable. Active mixing is associated with diatom dominance, followed by *Noctiluca* when the mixing slackens, making use of the available nutrients and supported by regenerated production. The bloom dynamics is explained for pre-bloom, bloom and post-bloom conditions with measurements on nutrients and plankton assemblages. The Noctiluca bloom (mid-March) is succeeded

* Corresponding author.
E-mail address: smitha@cmlre.gov.in (S. B.R.).
[1] Postal address: Centre for Marine Living Resources and Ecology, Ministry of Earth Sciences, LNG Road, Ochanthuruth (PO), Puthuvype, Kochi-682 508, Kerala, India.

https://doi.org/10.1016/j.scitotenv.2021.151173

by *Trichodesmium* (April–May), in the stratified nutrient depleted, abundant light environment and propagated southwards. Observed increasing trends in the SSHA over the period indicate strengthening of stratification and hence altered production patterns in the NEAS.

1. Introduction

Seasonal reversal of monsoon winds and the surface ocean circulation patterns regulate biological production in the Eastern Arabian Sea (EAS), with the summer monsoon upwelling dominant over South Eastern Arabian Sea Ecosystem (SEAS) and the winter cooling and convective mixing influencing the North Eastern Arabian Sea Ecosystem (NEAS). Besides, mesoscale processes such as cold/warm core eddies, meanderings etc. exert a profound influence on the ecosystem processes and associated biogeochemical cycles.

The upper layer of the tropical/lower subtropical oceans in general support high biological production as surface nutrient availability is maintained through dynamical processes that churn the water column, such as upwelling, convective mixing, horizontal advection, eddies/meanders etc. (Dugdale and Goering, 1967). The dynamics and production patterns of the EAS are strongly influenced by the Summer Monsoon (SM) extending from June to September and the Winter Monsoon (WM) from November to February. These two dominant seasons are inter-spaced by the Fall Inter Monsoon (FIM) in October and the Spring Inter Monsoon (SIM) from March to end May. Compared to other ecosystems of the EAS (South Eastern Arabian Sea and Lakshadweep Sea) the annual average Primary Productivity (PP) in NEAS (0.776 ton C/km^2/d) is relatively higher (Sanjeevan et al., 2011) both during the SM and WM seasons. SM production in NEAS is supported by open ocean upwelling or Ekman divergence north of the Findlater jet and through large scale horizontal advection of upwelled waters from the northern and western Arabian Sea (Kumar et al., 2001; Wiggert et al., 2000). High biological production during WM is supported mainly through convective mixing (Madhupratap et al., 1996; Banse and McClain, 1986; Wiggert et al., 2000) that bring nutrients to the surface from the base of the mixed layer (Banse, 1984; Kumar et al., 2001). During this season the oceanic region of NEAS is also hydrodynamically active, with eddies/meanderings and irregular flow patterns. During the SIM, low Sea Surface Temperature (SST < 25 °C) and deeper Mixed Layer Depth (MLD > 100 m) associated with WM are replaced by relatively warm surface waters (>26.5 °C) and shallow MLD (30–40 m) due to increase in solar radiation and slackening of northeast trade winds. However, high chlorophyll-*a* (Chl-*a*) (*av.* 0.81 mg m^{-3}) and primary production (*av.* 29.5 mg C $m^{-3}d^{-1}$) (Madhu et al., 2012) are sustained in the early phase of SIM also.

Past studies in the NEAS have documented the influence of convective mixing in enhancing biological production through 'new production' (*f-ratio*: 0.06–0.42) during WM. Production levels are sustained even during the WM-SIM transition period (Gandhi et al., 2010) through 'regenerated production' (f-ratio: 0.06–0.12). However, high f-ratio 0.37 and 0.42 during March 2004 and 2007 as reported by Gandhi et al. (2010) indicates that surface supply of nitrogen is maintained during SIM, which can be either due to an extended convective mixing process or any other processes that churn the water column thereby bringing nutrients to the surface.

Satellite imageries on ocean color for WM and early SIM show relatively higher production in the coastal waters and isolated pockets of high production in the oceanic regions of NEAS. Extensive algal blooms dominated by diatoms, dinoflagellates or by mixed algal groups are often associated with these high production areas (Dwivedi et al., 2015). Available explanations on the formation and spread of such blooms in NEAS during WM/SIM are based on convective mixing (Lotliker et al., 2018), iron-enrichment (Banerjee and Prasanna Kumar, 2014), land-based nutrient enrichment (Goes et al., 2005) etc. and do not adequately justify the occurrence of these blooms in patches or the associated species succession observed in such blooms. Here we attempt to explain these based on long-term observational data from FORV *Sagar Sampada*.

In situ observations from on-board the FORV *Sagar Sampada* (multiple cruises) indicate that the areas of high PP (bloom areas) vary both spatially and temporally across the coastal and oceanic regions. The occurrence of high production patches in the oceanic regions even during the SIM indicates the role of processes other than convective mixing in complementing their formation and sustenance. We ascribe this to mesoscale Cold Core Eddies (CCE) that promote oceanic upwelling. Based on in situ observations from a high production pocket at 21°20.38′N; 66°30.68′E, Smitha et al. (2013) documented that new production as stated in Gandhi et al. (2010) is sustained in the early phase of SIM (March) by a combination of convective mixing and CCEs. Warm Core Eddies (WCE) on the other hand, deepens the MLD by complementing the convective mixing process. Based on a suit of satellite and CMEM vertical profile, Xiang et al. (2019) states that stable stratification, surface cooling and excessive evaporation, contributed to the accumulation of *N. scintillans* cells in the study area. Additionally, high DIN:Si, together with long-term organic nutrient accumulation due to diatom blooms and terrestrial input of rich organic nutrients in the euphotic zone, provided the favorable conditions for *N. scintillans* to outcompete diatoms. Thus, large-scale *N. scintillans* bloom in surface water occurred under the conditions of upward convection and the presence of a cyclonic eddy.

We attempt to explain the occurrence and sustenance of isolated pockets of higher production in the open ocean of NEAS during the WM-SIM transition, by explaining the physical process associated with the CCE, the forcing mechanism leading to its formation, the Available Potential Energy (APE) associated with an eddy and its influence on the regional dynamics. Further, the massive bloom formation mechanism is explained based on in-situ observations. In brief, the manuscript is structured to explain; i) the intricate production pattern of NEAS during the winter-spring transition phase, ii) the contributory role of mesoscale processes in the upper layer production and iii) the massive *Noctiluca* bloom formation mechanism. We also provide details on the anticipated changes in the upper layer dynamics in response to the recent trends associated with climate change.

2. Data and analysis

Wind stress curl is computed from the u, v components of Scatterometer wind fields (daily) of ASCAT. Surface net heat flux is from the European Centre for Medium-Range Weather Forecasts (ECMWF) ORA-S3 (operational ocean reanalysis system of ECMWF). Chl-*a* and SST for the identification of the eddy are retrieved from GSFC NASA and processed using SeaDAS. 8-day composite of the Level 3-binned product for November to April for the years 2002–2019 derived from MODIS AQUA in 4 km resolution is used for the purpose. Sea Surface Height Anomaly (SSHA) is derived from Jason II as well as from the merged geophysical products from TOPEX/Poseidon and Jason I altimetry (10 days composite from November–April). Climatological values of Temperature and Salinity are taken from World Ocean Atlas (WOA). CCE is identified from satellite Chl-*a* imagery for March 2013 and in situ measurements along the eddy diameter (5 stations) were taken during the cruise-314 (SS314) of FORV *Sagar Sampada*. Continuous monitoring of surface meteorological parameters such as Air temperature, Atmospheric pressure, Wind speed and

direction in 15 min interval was done using the Automated Weather Station (AWS) onboard. Though vertical sampling extended up to 1000 m depth at each station, our analysis is restricted to the upper 300 m as the focus of the present study is on upper layer dynamics. Temperature profiles are from CTD (SBE Model 11 PLUS, Sea-Bird Inc.) in 1 m bin intervals. Bucket thermometer of make Theodor Friedrichs & Co. (scaling in 0.5 °C; accuracy ±0.5 °C) was used to measure SST in each station. At standard depths, salinity values from CTD were validated and corrected with the values derived from on-board Autosal (Guidline 8400). The surface nutrient analysis follows Grasshoff et al., 1983. MLD is taken as the depth at which σ_t values increase by 0.2 from surface value.

Vertical profiles of currents along the cruise track are derived from RDI 75 kHz Ocean Surveyor Acoustics Doppler Current Profiler (ADCP). The instrument was configured to 16 m bin size to obtain data from 30 to 500 m depth range with an ensemble interval of 2 s with the ringing of 8 m and transducer depth 5.6 m in broadband mode. The system was run via VMDAS, Vessel Mounted Data Acquisition Software and the data are post processed in WinADCP.

Phytoplankton samples were collected by filtering ~50 l (in non-bloom stations) of surface water through 20 μm bolting silk, and the filtrates were preserved in neutralized formaldehyde (1–3%) -Lugol's iodine solution. Qualitative and quantitative analysis of phytoplankton samples were carried out using a Sedgewick Rafter counting cell under a Nikon Eclipse microscope following standard identification keys (Tomas, 1997). In addition to these, past cruise data sets of FORV *Sagar Sampada* corresponding to the process and season, particularly profiles of CTD, primary productivity (C-14 uptake rates) and Chl *a* (Spectrophotometric measurements using a double-beam Perkin-Elmer UV–Visible spectrophotometer following 90% acetone extraction (Parsons et al., 1984)) are used to compare the properties associated with WCE/CCE/non eddy regions. In addition to this nutrient profiles and phytoplankton species information measured/collected during SS262, 263 and 264 are considered in the analysis to explain the different phases of biological production.

Eddy detection was done based on Okubo-Weiss (OW) parameter using Sea level anomaly (SLA) in 7 day temporal resolution from AVISO (https://www.aviso.altimetry.fr) for the period October 2012–March 2013 Okubo (1970) and Weiss (1991). The eddies are identified using SLA contours and geostrophic currents from geostrophic equations,

$$u = \frac{-g}{f}\frac{\partial h}{\partial y} \text{ and } v = \frac{g}{f}\frac{\partial h}{\partial x}$$

where u and v are the zonal and meridional components of geostrophic currents, g is the gravitational acceleration, f is the Coriolis parameter, x and y are longitudinal, latitudinal co-ordinates and h is the SSHA. Eddies are also tracked using the contours of OW parameter of two-dimensional velocity field V = (u,v), OW (Okubo, 1970; Weiss, 1991) and are defined as

$$OW = s_n^2 + s_s^2 - w^2$$

where s_n is the normal strain component, s_s is the shear strain component, and w is the relative vorticity.

$$s_n = \frac{\partial u}{\partial x} - \frac{\partial v}{\partial y} \quad (1)$$

$$s_s = \frac{\partial v}{\partial x} + \frac{\partial u}{\partial y} \quad (2)$$

$$w = \frac{\partial v}{\partial x} - \frac{\partial u}{\partial y} \quad (3)$$

Eddies are marked as the regions where vorticity dominate the strain. Closed contours of $W = -2 \times 10^{-2}\ S^{-1}$ are opted for defining the eddy following Chelton et al. (2007).

3. Results and discussion

3.1. Ecosystem processes during WM-SIM

It is well established that, during WM the cold, dry continental winds from north east promote negative heat flux or heat loss causing enhanced evaporation and increase in salinity across the upper ocean of NEAS (Kumar and Prasad, 1999). This leads to the sinking of the cold high saline surface water which is replaced by nutrient rich subsurface waters (convective mixing) leading to enhanced Primary Production (PP) (Madhupratap et al., 1996; Kumar and Prasad, 1999; Kumar et al., 2001; Wiggert et al., 2005). The extent and measure of the evaporative cooling and changes in density are well evident in the surface net heat flux, the monthly distribution of which has been analyzed based on ECMWF Ocean Reanalysis ORA-S3 for Oct-Mar (Fig. 1). Heat loss is maximum during December (of the order of 250 w/m^2), which is comparable to that reported by Kumar and Prasad (1999). The sharp gradational decrease in the heat loss south of 18°N and west of 60°E leads to spatial variations between east-west (250 to 95 w/m^2) and south-north (5 to 250 w/m^2). The distribution pattern of Chl-*a* is

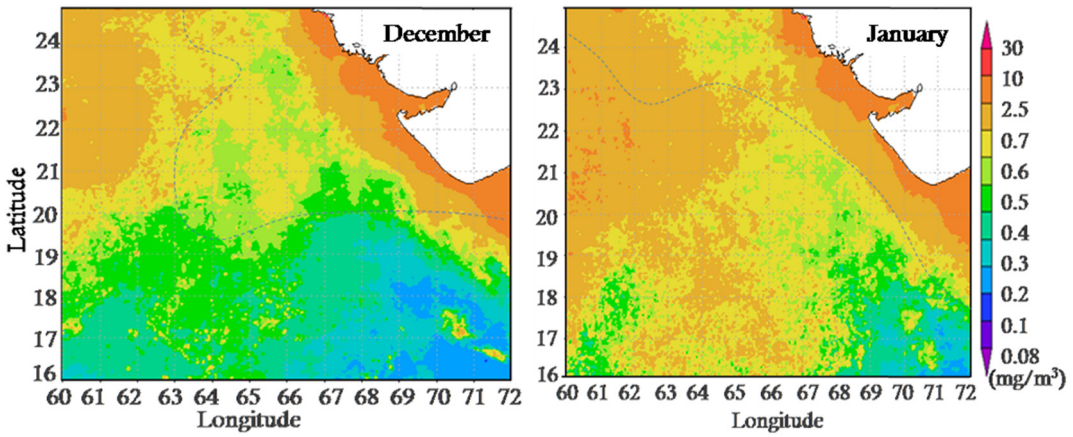

Fig. 1. Study area showing long-term climatology of Chl-*a* for December and January from MODIS AQUA with high productivity along the coastal belt and the northwest. Heat flux is more than 150 w/m^2 northeast of the dashed line. High productive waters propagate southwards during January.

Table 1
In-situ observations on MLD, Surface Chl(S-Chl-*a*) and Column-Chl (C-Chl-*a*) in the CCE, WCE, non- eddy region & coastal areas from cruise data of FORV Sagar Sampada. Cruise number is given in brackets at Column-1. The values indicate the average of the observations made (number of observations in bracket) in the region. Eddy/non eddy regions are identified based on SSHA and geostrophic currents from TOPEX/Poseidon.

Month/year	CCE (Avg)			WCE (Avg)			Non-eddy (Avg)		
	MLD (m)	S-Chl (mgm^{-3})	C-Chl (mgm^{-2})	MLD (m)	S-Chl (mgm^{-3})	C-Chl (mgm^{-2})	MLD (m)	S-Chl (mgm^{-3})	C-Chl (mgm^{-2})
Nov 1998 (SS169)	40 (9)	0.48 (9)	35.18 (9)	–	0.35 (rs)	–	39 (2)	0.30 (2)	11.70 (2)
Dec 2000 (SS190)	33 (2)	1.29 (2)	54.93 (2)	–	0.55 (rs)	–	52 (2)	0.53 (2)	25.50 (2)
Jan 2002/2003 (SS199& 211)	23 (2)	1.75 (rs)	–	90 (10)	0.65 (rs)	–	53 (2)	0.75 (rs)	–
Feb 2009 (SS262)	23 (3)	1.32 (3)	38.67 (2)	100 (3)	1.88 (3)	53.53 (3)	69 (2)	0.78 (2)	38.46 (2)
Mar 2000/2013 (SS182&314)	26 (11)	0.57 (6)	34.23 (6)	44 (2)	0.48 (2)	20.5 (2)	61 (2)	0.29 (2)	16.10 (2)

uniform for the Northeastern part of the study area and spreads southwest with the progress in season (Fig. 1).

Influence of air-sea coupling in terms of the evaporative cooling and sinking of surface waters, on the upper layer processes is easily traceable in the surface Chl - *a* distribution. Density driven convective mixing associated with the winter cooling of NEAS, possibly push the MLD down to 40–70 m (Table 1). Active convective mixing regions, therefore are expected to be homogeneously nutrient rich and productive. Madhupratap et al. (1996) reported a general increase in biological productivity as a result of the winter cooling and the convective mixing processes. On the contrary, monthly climatology for the surface chlorophyll for December and January shows pockets of high production associated with shallow (10 to 25 m) or deep (75 to 106 m) MLDs. Other than the coastal waters with Chl $a > 2.5$ mg/m^3, only the northwest of the study region shows high production, >1 mg/m^3, with scattered patches southwards. This spread further southwards during January, again in patches, eventually making the entire region highly productive. The occurrence of high production pockets, especially in the offshore waters, suggest the complementary role of forcing mechanisms or processes other than convective mixing that perhaps enhance nutrient supply to the upper layer.

The geostrophic imbalance caused due to basin-scale evaporative cooling associated with the prevailing cold, dry north easterlies may cause abrupt irregularities in sea level pressure. The flow instability results in unorganized flow patterns in surface waters (Fig. 2) with associated changes in the Sea Surface Height (SSH). Concurrent observations on surface Chl-*a* and SST from MODIS AQUA show low/high SST and enhanced productivity patches associated with divergence/convergence or areas of negative/positive sea level indicating the role of mesoscale processes specifically the cold/warm core eddies.

3.1.1. Cold/warm core eddies

The eddy regions are identified based on its characteristics of low and high sea level in the core, the critical point in the velocity field in the core and the negative value in the OW parameter. OW is the most widely used threshold- based method as this compares the relative vorticity to strain, which tends to be true in the inner part of the eddy. The inner region of an eddy will have negative OW value and so the inner boundary, including the eddy's core is identified based on negative OW value (Fig. 3). That is the eddy regions are identified based on the OW, considering closed contours of $W = -2 \times 10^{-12}\ s^{-2}$, which indicates the region of vorticity as the leading component than the two strain components, normal and shear. While the outer boundary of the eddy is identified based on current speed thresholds, which is derived based on the SSHA derived geostrophic currents.

WCE/CCE's are delineated based on the SST gradients in high/low sea level (+ve/−ve SSHA) areas with the circular surface flow in the anticyclonic/cyclonic direction. Eddy interior is assumed as the region where the magnitude of SST gradient increases/decreases radially towards the centre. Eddy limits are defined as the outermost closed isothermal line around the eddy. These are compared with that of the OW estimates.

The eddies identified include both propagating and stationary (Fig. 4). The tracks of propagating eddies are determined by comparing the cool pools of low sea level in successive time steps of 8 days. An eddy is identified as stationary if the new position does not change the location grid of $0.25 \times 0.25°$ in successive time steps. On the other hand, if the feature is not observed in the source grid, either it is decayed or identified as a propagating disturbance. The same is confirmed again with SSHA and the OW in the different temporal domain. The analysis is repeated with weekly data for

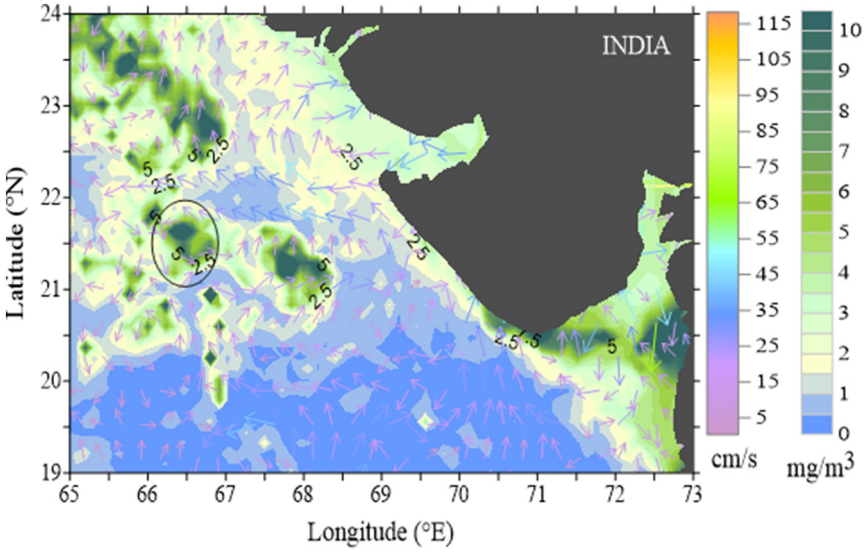

Fig. 2. Chl- *a* (mg/m^3) imagery from MODIS AQUA showing Cold core eddy CCE6b (−circled area) overlaid with Jason II Altimetry derived geostrophic currents (cm/s) for 9th March 2013.

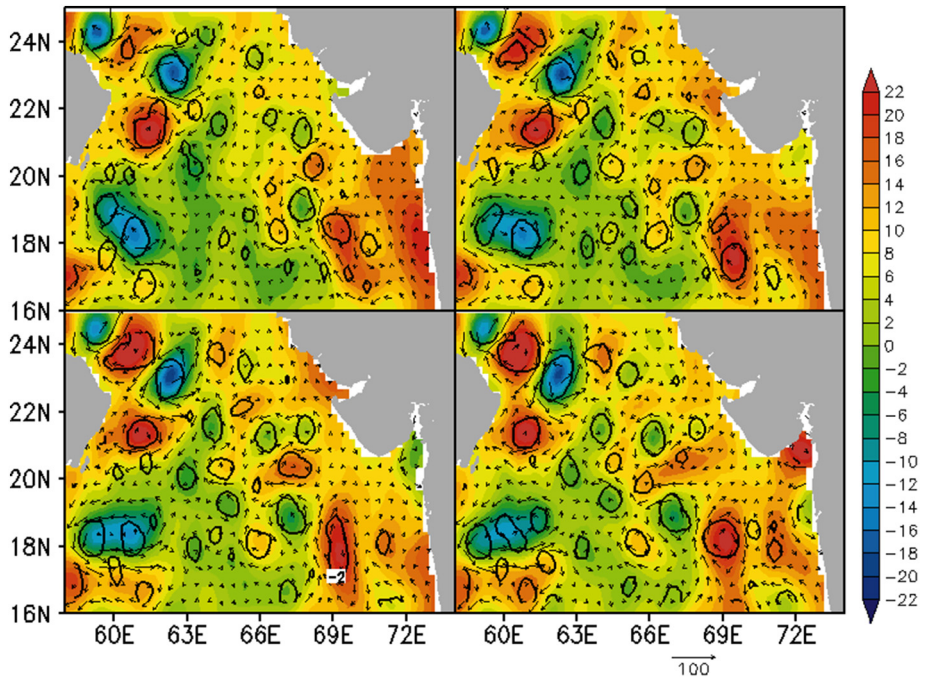

Fig. 3. SSHA and OW closed contour for the first (a), second (b), third(c) and fourth (d) week of March. The NEAS is observed with number of cyclonic (cold core) and anticyclonic (warm. core) eddies resulting retention areas and high export flux in the region.

2003 to 2019, and the recurring processes tagged are confirmed with the climatological average.

3.1.2. Mechanism of formation of WM-SIM eddies in NEAS

An eddy can be cyclonic or anticyclonic, causing divergence/convergence and cooling/warming in SST that ultimately influences the biogeochemistry of the region. The possible mechanisms triggering eddy formation is studied using in-situ and satellite measurements during March 2013 for a selected eddy (eddy 6b in Fig. 4). Of the possible mechanisms driving the eddy formation, daily wind stress curl (Pond and Pickard, 1993) derived from ASCAT wind field, validated with the available wind measurements from the AWS on-board (has records in every 15 min) is analyzed for the observation period using the formula;

$$\text{Curl} = \frac{\Delta\tau_y}{\Delta x} - \frac{\Delta\tau_x}{\Delta y} \quad (4)$$

where, τ_x and τ_y are the x and y components of wind stress, respectively.

Cyclonic/anticyclonic flows associated with wind stress can be easily distinguished by the sign of the wind stress curl. Positive/negative curl shows mass transport directed perpendicular to the applied stress to the right/left and indicate divergent/convergent flows. For the present observation, the flow is divergent and cyclonic, but concurrent observation on the atmospheric wind curl gives negative values (-3.05×10^{-7} to 0.86×10^{-7}). This implies that wind stress curl does not play a significant role in the rotational motion observed in-situ, thereby ruling out the role of wind in the initiation and sustenance of divergence that maintains the cyclonic flow. The isotherms and the current patterns confirm the existence of cold core eddy in the region, but the wind curl is non-supportive to the existence of the eddy. This shows that wind or wind curl is not the actual forcing mechanism triggering this cold core eddy.

Another possibility of topographic steering or the occurrence of mesoscale processes over mountain ranges or ridges on the ocean floor is also ruled out as the depth of the study area is more than 2000 m. Chance of pinching off of the eddy from boundary current is also not likely as the region do not show any strong organized boundary flow patterns during the season. Another possibility is the occurrence of instabilities, either baroclinic or barotropic generally observed in the deep ocean due to the mixing of water masses with different densities. The water masses in the upper layers (~1000 m) in the Arabian Sea include Arabian Sea High Saline Water (ASHSW) (surface-100 m), Persian Gulf Water (PGW) (200–400 m) and Red Sea Water (RSW) (500–800 m) (Shetye et al., 1994; Kumar and Prasad, 1999). In the tropical/lower subtropical region, flow in the ocean interior is generally baroclinically unstable and therefore generates meanders and eddies that transport mass, momentum and heat. Such disturbances or eddies will be in the scale of the order of baroclinic Rossby Radius (Rd), a natural scale of the ocean associated with eddies, fronts, boundary currents etc. Baroclinic instability acts on horizontal scales larger than

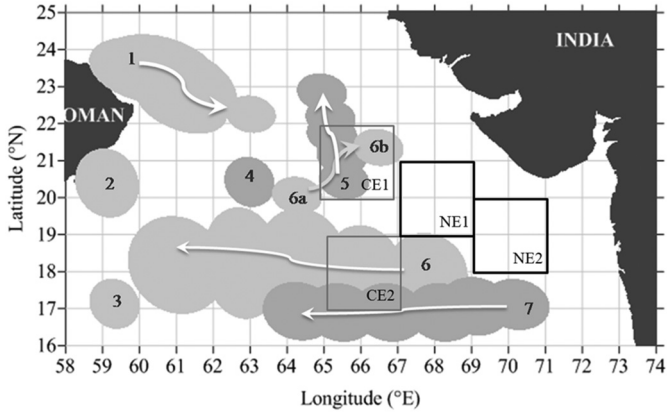

Fig. 4. Schematic diagram showing cold core eddies (1 to 7) identified based on long term data sets on SSHA (Altimetry), SST and Chl-*a* (from MODIS AQUA). Arrows shows the propagation path of the eddies. Boxes CE1 & CE2 are eddy regions selected for the analysis of surface and column Chl-*a*. NE1 & NE2 represents non-eddy regions selected for comparisons. Detailed analysis is exercised for eddy 6b based on in-situ observations along its diameter from onboard FORV Sagar Sampada during cruise 314 (March 2013).

deformation radius and the Rd is estimated as NH/f, where f is the Coriolis parameter, N the depth averaged Brunt-Vaisala frequency (BV) and H, depth (Gill, 1982).

Where, BV is represented as N^2 and derived as

$$BV = \frac{-g}{\rho}\left(\frac{\partial \sigma_t}{\partial z}\right) \quad (5)$$

Here, g is the gravitational acceleration, z is the depth, σ_t is ρ-1000 and ρ is the density of sea water (Turner, 1973; Narasimha Rao, 2002).

Associated with an eddy like physical processes, potential energy, manifested by the perturbation of the density surfaces relative to horizontal level surfaces, available for conversion into kinetic energy is referred to as the APE. APE is an index to address the energy distribution associated with such disturbances. APE associated with the eddy is estimated following, Kumar et al. (1992) as;

$$APE = \int_v \frac{1}{2}\rho_r (N)^2 \xi^2 dv \quad (6)$$

where, ρ_r is the density of reference state, which is computed based on the equation of seawater properties (Fofonoff and Millard, 1983) from objectively analyzed mean monthly temperature and salinity taken from World Ocean Atlas in 0.25° resolution. N is Brunt Vaisala frequency (BV), ξ is pressure displacement between two surfaces viz. measurement point and reference point. In addition, the Eddy Kinetic Energy (EKE) is calculated ($EKE = 1/2\,(u^2 + v^2)$) for the vertical section, and found that, the EKE dominates over APE in the core depth (20–90 m) of the eddy by 52%. The EKE is dominant in the eddy core (Avg 12.95 m^2/s^2). Also, the Rd computed (55 km) is less than the observed eddy diameter (120 km), indicating the baroclinic instability as the triggering mechanism of the eddy.

The distribution of APE calculated up to 275 m shows maximum (2.82 J/m^3) at the centre of the CCE between 100 and 225 m water columns. Average APE for the column at the centre is 0.615 J/m^3. While for the eastern flank the column values range between 0.27 and 0.55 J/m^3, it is only 0.18–0.27 J/m^3 for the west the less mixed area, where the currents are also weaker. Minimum APE in the west also coincides with the shallow MLD (18–20 m) and deeper euphotic zone (40–46 m). The higher energy part is more dynamic and is expected to support higher production.

Analysis of SLA for 21–22.2°N and 66–67°E for the years 2003–2019 indicate that the eddy appears annually during February–March and has a short life span of 1–3 months. During 2013 it was for a short period of nearly two months from 10th February to 5th April. Surface meteorological parameters showed the existence of cool (24.9–27.5 °C) and relatively dry air (Humidity; 74–82%) with northeasterly to southeasterly winds of magnitude varying between 2.6 and 5.6 m/s. SST varied between 25.5 and 26.5 °C with a considerable diurnal variation.

Based on the hydrography of the region, it is most likely that the instability is caused due to the abrupt changes in the column T-S properties owing to the presence of water masses such as ASHSW at the surface (0–150 m) and PGW at 200–400 m with Arabian Sea Minimum Salinity Water (ASMSW) sandwiched between the two. Also, the possible role of coastally trapped Kelvin waves with its propagation path along the shelf/slope (Rao et al., 2010) as reflected in the SLA distribution with semi-annual periodicity needs to be explored further.

3.1.3. In-situ observations in CCE - 6b

CCE – 6b (Fig. 5) is a propagating eddy that is pinched off from CCE-6 and is identified real time, from ocean color imagery as a mesoscale eddy approximately 120 km in diameter centred at 21°20.38′N; 66°30.68′E with a fall in sea level by 5 cm. The in-situ observations at CCE6b during March 2013, show a cyclonic surface geostrophic current pattern with Chl-*a* > 8 mg/m^3.

Surface nutrient concentration associated with the eddy shows relatively high values of Nitrate (NO_3) at the centre (0.89 μM) and the western flank (0.92 μM). Silicate (SiO_4) and Phosphate (PO_4) follows the same trend and measures 0.49 μM & 0.69 μM respectively at eddy centre and 0.47 μM & 0.64 μM for the western flank. For the eastern flank, the average concentrations were 0.08 μM, 0.12 μM and 0.43 μM for NO_3, SiO_4 and PO_4respectively. Subsistence of the eddy streamer at west is evident in the physical environmental setup, like current pattern, the thickness of the ML, weak mixing in terms BV and extended

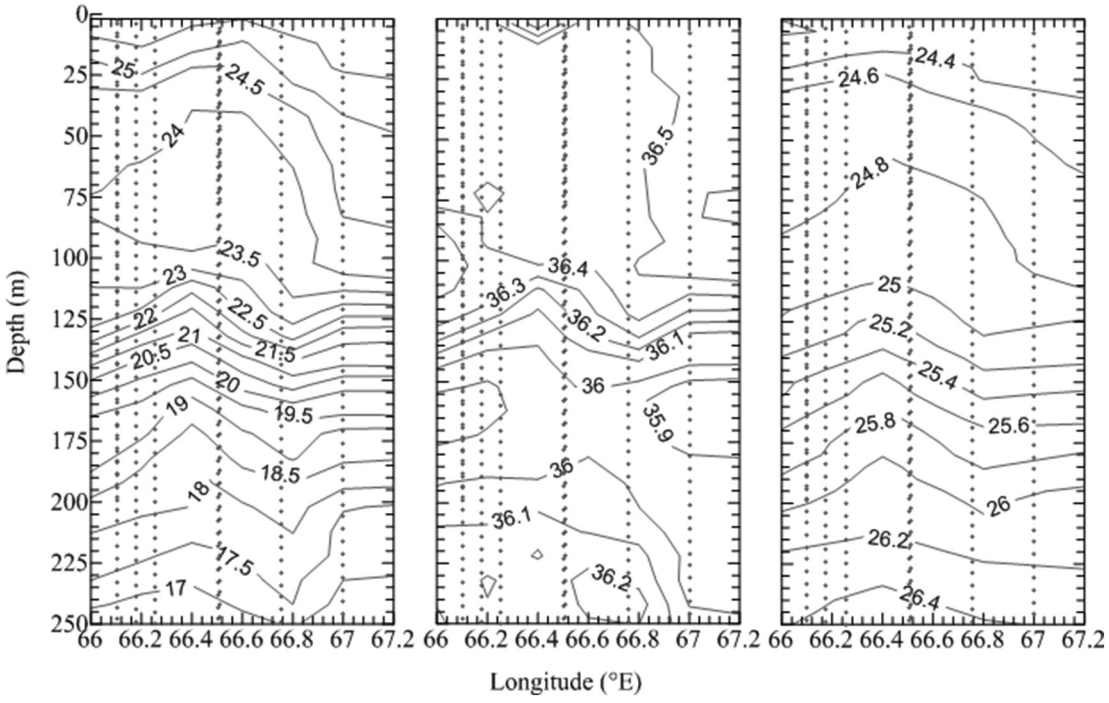

Fig. 5. Vertical section of (a) temperature (°C), (b) Salinity (psu) and (c) Sigma-t (kg/m^3) from CTD along the eddy diameter. The transect comprises 5 stations. CTD casts are oriented in a northeast to the southwest direction (66–67.2E longitude). Dotted lines indicate the location of CTD casts. (Reproduced from Smitha et al., 2013).

euphotic depth. The nutrient pattern with high concentrations at the centre and western flank indicates an aggregating behavior at the streamer, which is evident in the eddy associated biological response.

T-S properties show that the upper column is occupied by the ASHSW with its distribution slightly disturbed by the divergent flow associated with the eddy. The divergence associated with the cyclonic flow results in upwelling of subsurface waters, as is evident in the observed vertical thermal profiles of CTD (Fig. 5). Vertical sections of temperature derived from CTD (Fig. 5a) show maximum upsloping of 24 °C isotherm at 21°20.38′N; 66°30.68′E, corresponding to the core of the eddy. The upsloping was prominent at sub-surface (200–12 m) thereby shifting the D24 (depth of 24 °C isotherm) from 108 m to 45 m in the core and lowering the ambient temperature by 1 °C. Upsloping resulted in thinning of MLD to 11 m at the core while it was between 18 and 20 m in the western and 40 m in the eastern flanks of the CCE. Distribution of salinity (Fig. 5b) in the column shows the occurrence of high saline (36.5 psu) waters up to 108 m depth along the eastern flank whereas 36.4 psu saline waters extend up to 100 m in the core and western flank of the eddy. The isopycnal ($\sigma_t = 24.6$ kg/m^3) is shallow (25 m) in the core and western side of the eddy and is deep (65 m) along the eastern side. This indicates that the dense upwelled waters from the core flow to the western flank which explain the shallow MLD and high nutrient content observed along the western flank of the eddy despite its low APE.

Temperature and σ_t (Fig. 5c) properties indicate relatively weak mixing in the western flank of the eddy. The flow field associated with the CCE is depicted in Fig. 6. The current pattern shown is the representation of average velocity for 16 m bins or columns from 24 to 396 m along the eddy diameter in the northeast to southwest direction. The data is screened for noises identified by reviewing the Echo Intensity, Correlation and Percentage good (PG) values in the field 4. Besides, velocity reasonableness is reviewed for bin to bin and ensemble to ensemble, thereby confirming smooth transition for all the data considered for the analysis. Playback verification is done for the entire transect, and abrupt variations in the current sticks were removed before the analysis. Also, data are removed wherever sudden changes occurred in the course and speed of the vessel.

In the eastern flank of the CCE, the currents are stronger (0.2–0.6 m/s) and are directed northwards. While in the western flank, the strength is relatively weak (0.2–0.4 m/s) and is directed to the south. At the centre of the transect, which represent the eddy core, the flow velocity is near zero. Vertically, the current pattern is almost uniform, in both magnitude and direction, up to ~170 m (up to the 6th bin of the ADCP). Below this, the magnitude gets weaker but the flow pattern remains the same explaining uniform cyclonic (anticlockwise) flow up to almost 200 m depth, which is stronger in the east than its western counterpart.

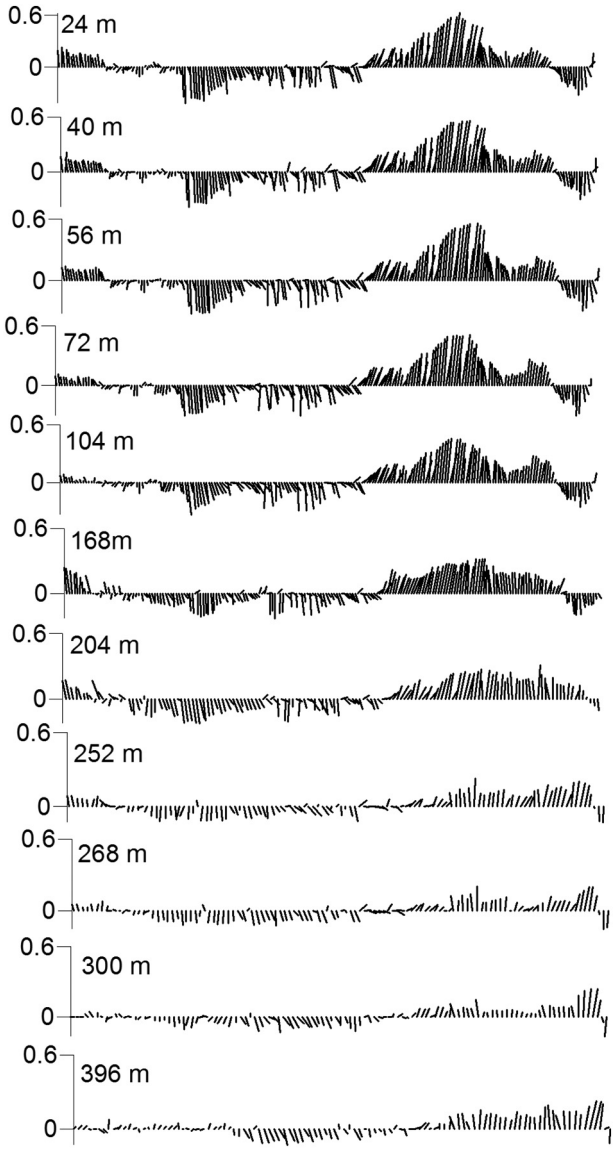

Fig. 6. Vertical profile of currents along the eddy diameter from ADCP measurements. The transect is aligned in a northeast to southwest orientation (66–67.2E longitude). Care is taken to remove the profiles at stations to avoid errors due to sudden changes in heading and speed of the vessel. (Reproduced from Smitha et al., 2013).

3.2. CCEs complement biological production

Explanations on the extensive blooms of algae recorded in the NEAS during the winter-spring inter monsoon transition period is attempted based on observations during 2011 on-board FORV cruises SS284, 285 and 286. Strong convective mixing in winter season enhances surface nutrient supply that sustains multi-species phytoplankton abundance with massive blooms of pennate diatoms such as *Haslea* spp. As the season progresses a more diverse community of centric diatoms, which can thrive even in less nutrient conditions dominate the mixed blooms. Higher SST and less turbulent conditions that prevail during the SIM season support the proliferation of the dinoflagellate *Noctiluca scintillans* which form massive blooms.

Primary production during WM in NEAS is in general supported by convective mixing, with CCEs complimenting the process in the offshore high production pockets. The WM production patterns and corresponding MLDs exhibit significant spatio-temporal variability (Table 1). The influence of CCEs on the production rates of the study area are addressed based on the monthly average data for four selected boxes of $2° \times 2°$ grid; 2 in eddy (CE1 & CE2) region and 2 in non-eddy (NE1 & NE2) region [CE1-65°-67°E; 20°-22°N, CE2-65°-67°E; 17°-19°N, NE1-67°-69°E;19°-21°N and NE2-69°-71°E; 18°-20°N] as shown in Fig. 4. Observations from the present study indicate that the production levels and micro-algal compositions in NEAS differ between the non-bloom area, CCE with uniform APE, CCE with non-uniform APE (CCE-6b) and the WCE areas. Whereas higher production levels in WM with mixed algal blooms are maintained by the convective mixing process and CCEs with uniform APE, the green *Noctiluca* dominated blooms are most often associated with WCEs and CCEs with non-uniform APE.

Enhanced WM productivity and associated bloom formation in NEAS starts in November, peaks during December, January & February, falls to values close to November production by March and disappear by April (Table 1). In the initial phase (Nov.), signatures of convective mixing are evident from the MLD (~40 m both in the eddy & non-eddy regions) and elevated surface and column productions. Higher surface & column Chl-*a* value in the CCE (0.48 mg m^{-3} & 35.18 mg m^{-2}) as against the non-eddy regions (0.30 mg m^{-3} & 11.70 mg m^{-2}) indicates that upwelled CCE waters have reached the

40 m depth which corresponds with the base of convective mixing. The elevated surface nitrate levels in the CCE (0.89 μM for CCE & 0.08 μM for non-eddy areas) support this view. Average microalgal concentration was 24×10^3 cells L^{-1} consisting mainly of diatoms (96.74%) and dinoflagellates (3.14%). Dominant diatoms were *Rhizosolenia hebetata* (33.6%), *Chaetoceros lorenzianus* (19.5%), *Nitzschia longissima* (12.8%), *Pseudo-nitzschia seriata* (8.8%) and *Thalassiothrix longissima* (6%). Dinoflagellates were composed mainly of *Noctiluca scintillans* (35.5%), *Protoperidinium oceanicum* (21.1%), *Ceratium sp.* (14.5%) and other dinoflagellates (13.2%).

The peak production in December, January and February in non-eddy areas is associated with enhanced convective mixing as evident from the deep MLDs (reaching 69 m by Feb). On the other hand, MLDs of CCEs reach shallow depths of 23 m by January/mid-February under the influence of strong Upsloping. In situ observations on surface & column Chl-*a* from the eddy and non- eddy regions (FORV *Sagar Sampada*) for November 1998 (SS169), March 2000 (SS182), December 2000 (SS190) and February 2009 (SS262) indicate that biological production in the CCE area on an average is two to three folds higher than in the non-eddy areas in all phases of the eddy. Average data for the eddy/non eddy regions are given in Table 1 against the corresponding cruise details and number of observations considered. Entire area irrespective of the presence or absence of an eddy is productive, obviously as a result of nutrient pumping by convective mixing/upsloping. However, in the active phase of the CCE (December to February) upwelled waters occupy the shallow MLD and provide more nutrients, thereby enhancing PP two to three folds than the non-eddy regions. Microalgae abundance is high (10,545 cells L^{-1}) and dominated by diatoms (96%) with dinoflagellates forming only 4% of the cell count. By mid-February/March the convective mixing slackens, and production rates fall. Though the cell numbers fall to 6208 cells^{-L}, the diatom dominance (91%) observed in the earlier months continue during March also.

Madhupratap et al. (1996) reported fairly high Primary production over a large stretch of the ocean north of 15°N, which would have otherwise remained oligotrophic as in the southern areas (SEAS). They reported the highest productivity in winter as 807 mg $Cm^{-2}d^{-1}$. This is less than that reported from active upwelling zones of northwestern Arabian Sea (Owens et al., 1993) during the summer monsoon (2500 mg $Cm^{-2}d^{-1}$), but approaches those reported from north Atlantic spring bloom (900–1200 mg $Cm^{-2}d^{-1}$). Biological parameters for the upper 120 m for February as reported in this paper show significant increase in values at 21°N; 67°E (eddy region) compared to that at 21°N; 64°E (Non-eddy region). For Chl *a*, the values reported are 34.4 & 18.9 mg m^{-2}, PP, 807 & 643 mg $Cm^{-2}d^{-1}$, and mesozooplankton (ZP) biomass 86 and 64 ml per100m^3. Relatively decreased abundance of Picoplankton (PCP) [16–22 & 4–27 $\times 10^3$ ml^{-1}] and almost similar trend in microzooplankton (MZ) counts [0.1–1 & 0.1–0.8 $\times 10^2$ l^{-1}] are also noted from this observation. Lathika (2015) reported phytoplankton standing stock (numerical abundance) and average phytoplankton cell density of 4×10^5 Cells/L in the open ocean waters during winter-spring observations. Diatoms form the predominant group, taking advantage of the rapid pumping of nutrients due to convective mixing. In general, the coastal region was dominated by *Chaetoceros lorenzianus*, *Chaetoceros* spp., while the oceanic region was dominated by *Rhizosolenia hebetata*. Other centric diatoms notable was *Thalassiosira* sp., observed in single cells, chains and in mucilaginous colonies, *Leptocylindrus* spp., *Guinardia* spp. etc. Pennate diatoms such as *Navicula directa*, *Haslea* sp., *Nitzschia longissima* and *Cylindrotheca closterium* were observed as monospecific proliferations and sometimes associated with *Noctiluca scintillans*.

Unlike the CCEs discussed above (CCE with uniform APE) the microalgal composition of CCEs with non-uniform APE [CCE-6b-a short-lived (2 to 3 months) propagating eddy that is pinched off from CCE-6] is however different. The western flank of this eddy is relatively calm due to low APE and harbor intense blooms of the green *Noctiluca scintillans* with cell numbers reaching 5.8×10^6/l (March 2013) and contributing as much as 97.8% of the microalgae standing stock. The remaining 2.2% is composed of diatoms. Surface Chl-*a* is as high as 13.25 mg m^3.The core of eddy also has high production rates with Chl-*a* value of 4.35 mgm^{-3} and cell counts of 5.8×10^4 L^{-1} dominated by dinoflagellates (94.5%). On the eastern flank of this eddy cell counts are much less (421 cells L^{-1}) and again dominated by dinoflagellates (77.9%) and diatoms (22.1%). Within the eddy, highest nitrate levels (0.92 μM) were seen in the western flank, which indicates that the upwelled waters from the core of the eddy flow westward and that some amount of nitrate is regenerated. It is known that stability of the water column (Tada et al., 2004), cold waters (Gomes et al., 2008a,b) and active phagotrophy (Sriwoon et al., 2008) promotes proliferation of green *Noctiluca*, a mixotrophic dinoflagellate. The available data indicates that diatoms thrive in the upwelled waters in the core and the eastern flanks of the eddy in the initial phase of the eddy formation and that the westward displacement of the core waters and the circular motion of the eddy result in the accumulation and retention of diatoms in the calm western flank. Noctiluca feed by phagotrophy on these diatoms and multiplies rapidly through vegetative reproduction. The bloom slowly spread to the core and the eastern flank. The mesozooplankton biovolume in the mixed layers of the core (1.09 ml m^{-3}) eastern flank (0.88 ml m^{-3}) and the western flank (0.22 ml m^3) agree well with these findings. Further, the findings of Dela-Cruz et al. (2008) that upwelling is the dominant mechanism that stimulates diatom bloom that in turn promote *Noctiluca* growth and the finding of Jang et al. (2010) that mesozooplankton abundance is strongly correlated with Noctiluca density as it is a strong competitor with mesozooplankton for food corroborate well with our observations.

Smitha et al. (2013), explained the biological response of CCE-6 and observed that the eddy core represents a dynamic system during the physically quiescent SIM with increased micro-algal abundance as well as higher Chl-*a* concentration (4.35 mgm^{-3}). This and suggests that the less turbulent flow pattern in the western flank of the eddy favored the aggregation of microalgae and formation of bloom patches, resulting in the occurrence of an intense bloom of green *Noctiluca* in the region. The physical and/or the environmental setup associated with the bloom also support the *Sverdrup paradigm* (Sverdrup, 1953; Platt et al., 1991) which explains that calm environment coinciding with deeper euphotic zone and shallow MLD may harbor microalgae bloom patches. Distribution of the surface nutrient pattern and the associated biological production, especially the intense bloom of *Noctiluca*, support the view that the observed regional bloom is supported by the CCE6b. The variability in the surface Chl-*a* and the phytoplankton community structure is recorded in many studies illustrating the species composition (Xiang et al., 2019) in bloom and non-bloom areas. However, the species composition or pigment analysis data are not available for the column to explain the Chl-*a* variability in the context of new production. Surfacing/settling of dinoflagellates especially the green *Noctiluca* during convective mixing/stratified conditions are discussed by Vidya and Siby (2018) and Xiang et al. (2019), however, still the details on the vertical distribution of phytoplankton/species composition in a cold core eddy or any region, where nutrient pumping is active supporting new production are unavailable.

The physical processes and biological interactions that promote and sustain the high productivity pockets (Spring *Noctiluca* blooms) in the offshore/deep-Sea waters of NEAS during the SIM season are mostly associated with WCEs. With the onset of WM, several CCEs and WCEs appear in NEAS (Fig. 4). With the advancing of WM, turbulent mixing inside the WCE intensify, pushing the MLDs to 100 m or more by the first half of February month. Deep mixing is known to limit PP and conserve nutrients (Bradford et al., 1982; Dufois et al., 2016). With the advent of SIM season (mid-Feb) trade winds slacken, and SST reach to >27 °C leading to strong surface stratification and reduced turbulent mixing which promote the formation of spring blooms of the green Noctiluca inside these WCEs. Details on the pre-bloom, bloom and post-bloom stages of a green *Noctiluca* bloom from January to April

2011 was captured through 3 consecutive cruises of FORV-SS (Fig. 7). Results from this study are discussed below;

During the pre-bloom phase (27th January to 12th February 2011), the Isothermal Layer Depth (ILD) was at 100 m with a deep MLD at 80 m and a Barrier Layer of 20 m thickness. Surface Chl-*a* in the WCE (Table 1) was close to the values recorded for non-eddy regions which implies that the vorticity of WCEs draws productive waters from non-eddy regions to the inside of the eddy. However, unlike CCEs, the WCEs in its active state are highly turbulent and do not support primary production despite being nutrient rich (NO_3 = 2.13 μM L^{-1}). Phytoplankton cell counts were low (2736 cell/L), represented by diatoms (80%) and dinoflagellates (19.2%). Dinoflagellate was dominated by the green *N. scintillans* (13%) whereas among the diatoms the unusual occurrence of *Rhizosolenia* (13%) was recorded. The vertically migrating *Rhizosolenia* mats appear to replenish the surface nutrient availability in the initial stages of the bloom formation. Mesozooplankton abundance was low (288 nos/m^3) dominated by copepods (91%), *chaetognaths* (3%) and *ostracods* (1%).

With the start of SIM season in mid-February, surface waters become warmer (>27 °C) and stratified with reduced silicate availability (1.26–1.81 μM L^{-1}), conditions that are less favorable to diatoms. The ILD shallows to 85 m with MLD at 50 m and a thick barocline layer of 35 m. Taking advantage of the conserved nutrients in the WCE and availability of diatoms as an initial food source, the mixotrophic green *Noctiluca* proliferates rapidly by binary fission to form a moderate spring bloom (14400cells/L). The bloom forming *Noctiluca* contribute to 93.4% of the total cell count (15 × 10^4 cells L^{-1}) in the study area composed of 96% dinoflagellates and 3% diatoms. Microzooplankton abundance stood at 1,202,500 nos/m^2 dominated by ciliates (68%). The numerical abundance of mesozooplankton was 1830 nos/m^2 dominated by copepods (96%). Chaetognaths formed 1% and ostracods 0.5%. Due to the bloom formation, surface nitrate levels fell to 0.29 μM L^{-1}, whereas NH_4^+ levels increased to 0.75 μM L^{-1}. Experimental studies (Collos et al., 2004) have documented that dinoflagellate prefer NH_4^+ as the substrate for production whereas diatoms prefer NO_3^-. However, studies by Singh et al. (2014) indicate that NO_3^- is preferred by both diatoms and dinoflagellates. Goes et al. (2018) studied growth rates in *Noctiluca* under controlled experimental conditions and found that urea is the most preferred N-source for *Noctiluca*, followed by NH_4^+ and that NO_3^- appears to be the least preferred source. In the instant case the nitrogen demands of the proliferating *Noctiluca* are expected to be met directly by using NH_4^+ as the substrate and/or using the NO_3^- produced by nitrifying bacteria through the oxidation of Ammonia as the substrate (regenerated production). Though we do not have the actual bacterial counts for the WCE, the presence of 68% ciliates in the microzooplankton indicates to the high abundance of nitrifying bacteria.

The post bloom phase or the crash stage begins in the first week of March and extends to the last week (3rd to 22nd March in the instant case). The MLD shallows to 30 m, the ILD is at 40 m and the thickness of the barrier layer was only 10 m. Surface nitrate and ammonia levels increase to 0.32 μM L^{-1} and 1.85 μM L^{-1} respectively. Phytoplankton cell count increases to 31,1866 nos/m^2, dominated by diatoms (99%) with *Noctiluca* forming only <1% and the blue-green algae *Trichodesmium erythraeum* < 0.01% of the cell count. The *Noctiluca* bloom crash during this period and sink down in the form of POM. Bacteria act on the POM and produce ammonia and nitrate which sustains the regenerated production dominated by diatoms. However, the microzooplankton count is reduced to 365 nos/m^2 dominated by ciliates (71%) and a similar decreasing trend is observed in the mesozooplankton count (365 nos/m^3) as well, with copepods forming 76% of the cell count. Unlike other bloom years, the 2011 bloom had zero representation of ostracods and only 3% of chaetognaths. On the other hand, in the bloom year 2009, the post-bloom biomass of mesozooplankton in early March was composed of ostracods (28%), chaetognaths (10%) and copepods (45%). In the late stages of the post-bloom (end March) ostracod numbers increased to 39% of the mesozooplankton biomass. Expectedly the higher phytoplankton abundance in the early stages of post-bloom stage are sustained through re-generated production. However, as the season progresses the increasing

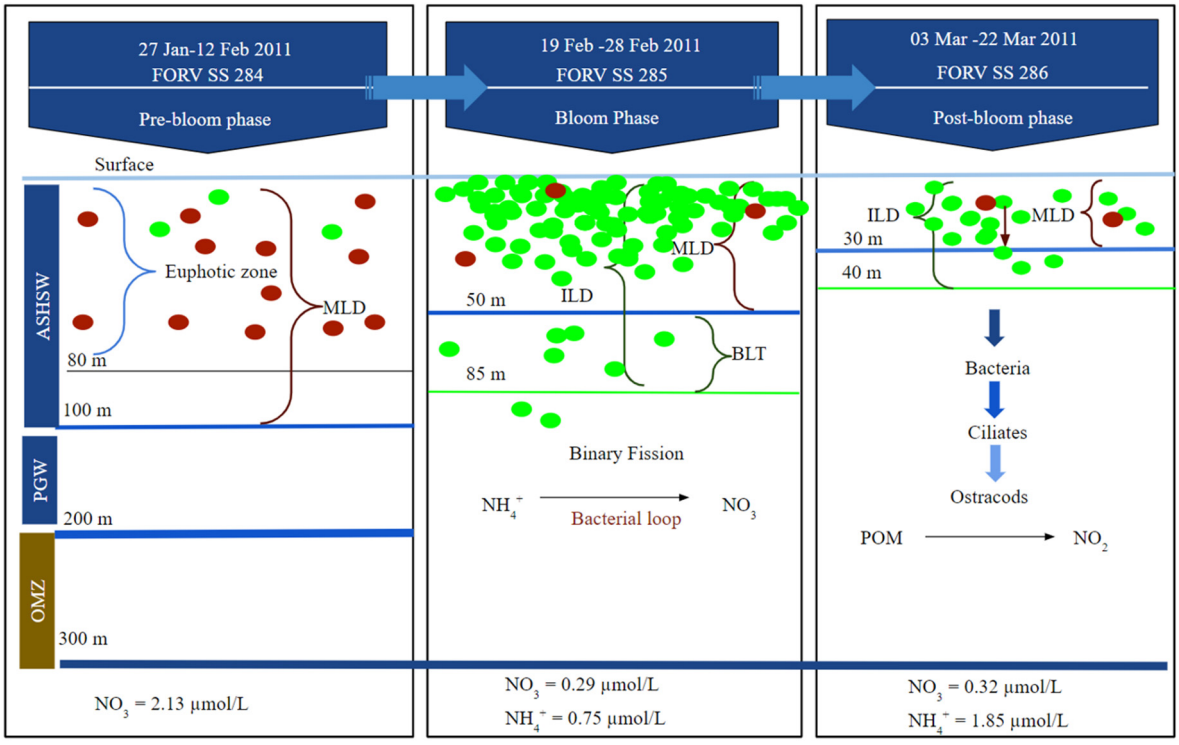

Fig. 7. Schematic representation of the process associated with the blooming of Noctiluca in the NEAS during winter-spring. The green circles represent Noctiluca cells. Red circles denote diatom cells. The representation is done based on the FORV SS observations during 2011, and the available secondary information.

ciliates devour most of these bacteria leading to a sharp fall in nitrate production. Ciliates in turn are consumed by the ostracods and chaetognaths. The end of post-bloom phase is marked by highly reduced phytoplankton counts (<300 nos/m^2) and surface nitrate levels (<0.1 μM L^{-1}).

By the end, March/early April the equatorial WICC transport these oligotrophic waters southward to areas where the SST is higher and the surface waters contain more iron, conditions favorable for the few blue-green algae *Trichodesmium erythraeum* present in these waters to flourish through diazotrophy (Capone et al., 1998; Gomes et al., 2008a,b). The species is known as the 'biological indication' of stratification and nitrogen limitation in the ocean surface layer (Jyothibabu et al., 2017). *T. erythraeum* blooms are commonly observed in the offshore waters during the April–May period, whereas mixed bloom of *Trichodesmium* with *Noctiluca miliaris* are common during March–April (Sushma et al., 2012).

3.3. Long term trends in the NEAS upper layer

On a basin scale the Arabian Sea show a warming trend since 1960 at the rate of 0.10 to 0.12 °C/decade (Prasanna Kumar et al., 2009; Roxy et al., 2014). Dominant decadal cycle until mid-1990s and disruption thereafter are recorded in the past studies. The warming trend is higher in SEAS as compared to NEAS (Narvekar et al., 2017) due to the freshening in the former as a result of the intrusion of BoB water during the winter season. However, there is a significant disparity in trend between season, the Dec-Feb wind in the NEAS for long term records strengthening in the wind (Narvekar et al., 2017), while the Jan-Mar wind shows a weakening trend (Goes et al., 2020). There have not been much studies addressing the interannual variability, the extended or reduced duration and the biological implications of the changes. However, recent study from Vidya and Siby (2018), explains 50% reduction in Chl-*a* concentration in the region during the winter 2015–16, which is a strong El Nino year, compared to normal years. Also, phytoplankton marker pigments showed a 50% reduction in microplankton abundance, along with increased abundance in picoplankton during 2016 compared to a normal year, 2013.

In the present analysis, average SSHA during March in NEAS show an increasing trend by 10 cm (Fig. 8) during 1993 to 2019, possibly from an enhanced warming and consequent stratification of the upper layer (steric effect). This observation is consistent with the views of Gomes et al. (2014) that the Arabian Sea appears to be experiencing a shallowing of Mixed Layer, due to the weakening of winter convective mixing and winds which also has the potential to alter the WM microalgae composition in NEAS. Also, the analysis indicates significant inter-annual variability in the number and intensity of low and high pockets. These regional processes are observed to be correlated to the warm/cool phase associated with the El Nino/La Nina as is evident for the years 1997, 2002 (El Nino), and 1998 (La Nina). Another interesting observation from Boyce Daniel et al. (2010), that Chl-*a* trends, as

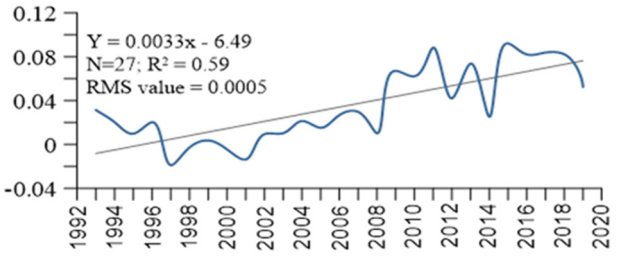

Fig. 8. Long-term trend in SSHA for 2 selected boxes in the NEAS for March centred at 21N; 65E and 22N; 66E. Y-axis represents SSHA in m against year in the x-axis. The data is from AVISO - DT MSLA - Merged Product - Up-to-date Global Processing. Figure shows an increasing sea level of about 10 cm.

continuous log linear functions of time, revealed phytoplankton declines in eight out of ten regions. Among these, the North Indian Ocean and South Indian regions were observed with an increase at the rate of 0.0018 ± 0.0015 mgm^{-3}/yr & 0.02 ± 0.0011 mgm^{-3}/yr respectively. Contradictory to this, Roxy et al. (2016) explains an alarming decrease of phytoplankton concentration by 20%, which is strongest during past 16 years (30%), in the 50–65E; 5–25N domain. The author explains the discrepancy with that of the earlier findings with the support of long-term data sets derived through Earth System models.

While addressing the physical settings associated with the Subsurface Chlorophyll Maxima (SCM), analysis from Midhun Shah et al. (2019) explain the warming trend in the March SST for the NEAS. Also, this gives indications to the possible strengthening of SCM in the scenario of warming and enhanced stratification. The sensitivity analysis (Global sensitivity Analysis) indicates that the warming trend in NEAS is resulting in the strengthening of the stratification, which in turn influences the concentration in SCM and is capable of altering the primary production. Warming may increase nutrient limitation due to strengthening in stratification, which results in a reduction in phytoplankton biomass and a shift towards a phytoplankton assemblage dominated by small phytoplankton (Li et al., 2009; Moran et al., 2010). So, the reason behind the shift observed in the phytoplankton composition and recurring occurrence of *Noctiluca* bloom from the recent past to be explored taking consideration of these factors too. In brief, the impact of warming/stratification in the primary production pattern is complex, as explained by Toseland et al. (2013), the response of warming can be direct and indirect. Increase in temperature may alter the N:P, in turn increasing demand for N with consequences for marine carbon cycle due to shift towards N limitation. The response can be reflected in altered species composition and production pattern, the explanation of which requires a comprehensive study linking physics to biogeochemistry to the ecophysiology and is beyond the scope of the present study.

4. Summary

The overall productivity of NEAS is comparatively higher during the WM, and early SIM as the winter cooling and associated convective mixing drives nutrients to surface waters. The present study establishes that pockets of high production and bloom formation in the oceanic regions of NEAS are most often associated with mesoscale eddies which occurs persistently as evident from the SSH anomalies and Okubo-Weiss parameters. Eddy core is dominant of EKE over the APE and the diameter of the observed eddy being wider than the Rossby radius it is suggested that the baroclinic instability is a possible mechanism for the eddy formation. These eddies have a life span varying from two to six months. CCEs with uniform APE are in general the sites of mixed algal blooms dominated by diatoms. However, CCEs with non-uniform APE promote intense blooms of the green *Noctiluca scintillans* on its calm fronts. With the onset of SIM season (mid -February), the WCEs begin to shallow, become less turbulent and promote the proliferation and blooming of *N. scintillans* using the nutrients conserved inside the eddy. These blooms are sustained till April through regenerated production. From April the oligotrophic surface waters of NEAS (North of 17°N) are transported southward by the WICC where the SST is higher, and the surface waters contain more iron. Under these conditions, the cyanobacteria *T. erythraeum* undertakes diazotrophy and form extensive blooms. Intense blooms of *T. erythraeum* have been reported from Ratnagiri (17°N) and Goa areas during April and May. Winter cooling and convective mixing in NEAS are reportedly showing an increasing trend from 2003 onwards, making the NEAS more productive. An analysis of the long-term trends in the SSHA of NEAS (1993 to 2019) indicates a positive trend which suggests strengthening in stratification and as a result enhanced Noctiluca blooms.

CRediT authorship contribution statement

Smitha B. R.: Conceptualization, Methodology, Data collection/analysis, Validation, Writing – original draft. **V. N. Sanjeevan:** Conceptualization, analysis, writing – review & editing. **K. B. Padmakumar:** Taxonomic identification, Writing – review & editing. **S. H. Midhun:** Data processing/plotting. **T. C, Salini:** Data processing/plotting. **J. K. Lix:** Data processing/plotting.

Declaration of competing interest

I/We have no conflicts of interest to disclose.

Acknowledgement

Authors are grateful to the Secretary, Ministry of Earth Sciences, and Director, CMLRE for supporting the work and for providing facilities onboard FORV *Sagar Sampada* for in-situ measurements. All the fellow participants of the cruise FORV SS314 are thankfully acknowledged. Authors are thankful to Mrs. Asha Devi C R. and Mr. Maneesh T.P. for the measurements/data on zooplankton and nutrients (FORVSS314) used in the manuscript. In-situ data from earlier cruises are obtained from FORV Data Centre in CMLRE. Chlorophyll data was retrieved from GSFC NASA. ASCAT Scatterometer wind field is obtained from NOAA. The TOPEX/Poseidon and Jason SSHA product is generated from the Merged Geophysical Data Record. Climatological values of Temperature and Salinity are taken from World Ocean Atlas. Acknowledge the help rendered by Ms. Sarah Webb for the English correction. Authors are thankful to the anonymous reviewers for the critical comments. This is CMLRE contribution 144.

Funding

Ministry of Earth Sciences (MoES), India

References

Banerjee, P., Prasanna Kumar, S., 2014. Dust induced episodic phytoplankton blooms in the Arabian Sea during winter monsoon. J. Geophys. Res. Oceans 119, 7123–7138.

Banse, K., 1984. Overview of the hydrography and associated biological phenomena in the Arabian Sea, Off Pakistan. In: Milliman, J.D., Haq, B.H. (Eds.), Marine Geology and Oceanography of Arabian Sea and Coastal Pakistan, pp. 217–303.

Banse, K., McClain, C.R., 1986. Winter blooms of phytoplankton in the Arabian Sea as observed by the coastal zone color scanner. Mar. Ecol. Prog. Ser. 34, 201–211.

Boyce Daniel, G., Lewis, Marlon R., Worm, Boris, 2010. Global phytoplankton decline over the past century. Nature 466 29 July doi: 10.1038, Nature 09268.

Bradford, J.M., Heath, R.A., Chang, F.H., Hay, C.H., 1982. The effect of warm-core eddies on oceanic productivity off northeastern New Zealand. Deep-Sea Res. 29 (12A), 1501–1516.

Capone, D.G., Subramaniam, A., Montoya, J., Voss, M., Humborg, C., Johansen, A., Siefert, R., Carpenter, E.J., 1998. An extensive bloom of the N2-fixing cyanobacterium, *Trichodesmium erythraeum*, in the central Arabian Sea. Mar. Ecol. Prog. Ser. 172, 281–292.

Chelton, D.B., Schlax, M.G., Samelson, R.M., de-Szoeke, R.A., 2007. Global observations of large oceanic eddies. Geophys. Res. Lett. 34, L15606. https://doi.org/10.1029/2007GL030812.

Collos, Y., Gagne, C., Laabir, M., Vaquer, A., Cecchi, P., Souchu, P., 2004. Nitrogenous nutrition of *Alexandrium catenella* (Dinophyceae) in cultures and in Thau lagoon, southern France. J. Phycol. 40, 96–103.

Dela-Cruz, J., Middleton, J.M., Suthers, I.M., 2008. The influence of upwelling, coastal currents and water temperature on the distribution of the red-tide dinoflagellate, Noctiluca scintillans along the east coast of Australia. Hydrobiologica 598 (59-75).

Dufois, F., Hardman-Mountford, N.J., Greenwood, Jim, Richardson, Anthony J., Feng, Ming, Matear, Richard J., 2016. Anticyclonic eddies are more productive than cyclonic eddies in sub-tropical gyres because of winter mixing. Sci. Adv. 2016 (2), e1600282.

Dugdale, R.C., Goering, J.J., 1967. Uptake of new and regenerated forms of nitrogen in primary production. Limnol. Oceanogr. 12, 196–206.

Dwivedi, R., Rafeeq, M., Smitha, B.R., Padmakumar, K.B., Thomas, L.C., Sanjeevan, V.N., Prakash, P., Raman, M., 2015. Species identification of mixed algal bloom in the Northern Arabian Sea using Remote Sensing techniques. Environ. Monit. Assess. 87, 51. https://doi.org/10.1007/s10661-015-4291-2.

Fofonoff, P., Millard Jr., R.C., 1983. Algorithms for computation of fundamental properties of seawater. Unesco Technical Papers in Marine Sciences. 44 53 pp.

Gandhi, N., Ramesh, R., Prakash, S., Kumar, S., 2010. Nitrogen sources for new production in the NE Arabian Sea. J. Sea Res. https://doi.org/10.1016/j.seares.2010.12.002.

Gill, A.E., 1982. Atmosphere-ocean Dynamics. Academia Press, New York, p. 321.

Goes, J.I., Thoppil, P.G., Gomes, H.D.R., Fasullo, J.T., 2005. Warming of the eurasian landmass is making the Arabian Sea more productive. Science 308, 345–347. https://doi.org/10.1126/science.1106610.

Goes, J.I., Al-Hashimi, K., Buranapratheprat, A., Gomes, H.D.R., 2018. Ecological drivers of Green Noctiluca blooms in two monsoonal-driven ecosystems. Global Ecology and Oceanography of Harmful Algal Blooms, Chapter 17 Ecological Studies. 232. Springer International Publishing AG, Springer Nature. https://doi.org/10.1007/978-3-319-70069-4_17 2018.

Goes, J.I., Hongzhen, T., do Rosario Gomes, H., Anderson, O.R., Al-Hashmi, K., deRada, S., Luo, H., Al-Kharusi, L., Al-Azri, A., Martinson, D.G., 2020. Ecosystem state change in the Arabian Sea fuelled by the recent loss of snow over the Himalayan-Tibetan Plateau region. Sci. Rep. 10, 7422. https://doi.org/10.1038/s41598-020-64360-2.

Gomes, H.D.R., Goes, J.I., Matondkar, S.G.P., Buskey, E.J., Basu, S., Parab, Sushma, Thoppil, P., 2014. Massive outbreaks of Noctiluca scintillans blooms in the Arabian Sea due to spread of hypoxia. Nat. Commun. 5, 4862. https://doi.org/10.1038/ncomms 5862.

Gomes, H.D.R., Goes, J.I., Matondkar, S.G.P., Parab, S.G., Al-Azri, A.R.N., Thoppil, P.G., 2008a. Bloom of Noctiluca miliaris in the Arabian Sea – an in-situ and satellite study. Deep-Sea Res. I 55, 751–765.

Gomes, H.D.R., Matondkar, S.G.P., Parab, S.G., Goes, J.I., Pednekar, S., Al-Azri, A.R.N., Thoppil, P.G., 2008b. Unusual blooms of green Noctiluca miliaris (Dinophyceae) in the Arabian Sea during the winter monsoon. Geophys. Monogr. Ser. 185, 347–363.

Grasshoff, K., Ehrhardt, M., Kremling, K., 1983. Methods of Seawater Analysis. Verlag Chemie.

Jang, M.-C., Shin, K.S., Jang, P.-G., Lee, W.-J., 2010. Relationship between environmental factors and short-term variations of mesozooplankton during summer in Jangmok Bay, south-east Korea Ocean. Polar Res. 32 (1), 41–52.

Jyothibabu, R., Karnan, C., Jagadeesan, L., Arunpandi, N., Pandiarajan, R.S., Muraleedharan, K.R., Balachandran, K.K., 2017. Trichodesmium blooms and warm-core oceansurface features in the Arabian Sea and the Bay of Bengal. Mar. Pollut. Bull. vol.121 (1-2), 201–215 2017.

Kumar, Prasanna S., Prasad, T.G., 1999. Formation and spreading of Arabian Sea high saline water mass. J. Geophys. Res. 104 (C1), 1455–1464.

Kumar, Prasanna, S., Babu, M.T., Rao, D.P., 1992. Energy and generating mechanism of a subsurface, cold core eddy in the Bay of Bengal. Indian J. Mar. Sci. 21 140-142p.

Kumar, Prasanna, S.P., Ramaiah, N., Gauns, M., Sarma, V.V.V.S., Muraleedharan, P.M., Raghukumar, S., Dileep-Kumar, M., Madhupratap, M., 2001. Physical forcing of biological productivity in the Northern Arabian Sea during the Northeast Monsoon. Deep-Sea Res. 48, 1115–1126 2018.

Lathika, C.T., 2015. Microphytoplankton community structure along the North Eastern Arabian Sea during Winter monsoon. Ph.D Thesis. Cochin University of Science and Technology, p. 218.

Li, W.K.W., McLaughlin, F.A., Lovejoy, C., Carmack, E.C., 2009. Smallest algae thrive as the Arctic Ocean freshens. Science 326, 539.

Lotliker, Aneesh A., Baliarsingh, S.K., Trainer, Vera L., Wells, Mark L., Wilson, Cara, Bhaskar, T.V.S.Udaya, Samanta, Alakes, Shahimol, S.R., 2018. Characterization of oceanic Noctiluca blooms not associated with hypoxia in the Northeastern Arabian Sea. Harmful Algae 74, 46–57.

Madhu, N.V., Jyothibabu, R., Maheswaran, P.A., Jayaraj, K.A., Achuthankutty, C.T., 2012. Enhanced chlorophyll a and primary production in the northern Arabian Sea during the spring intermonsoon due to green Noctiluca scintillans bloom. Mar. Biol. Res. 8 (2012), 182–188.

Madhupratap, M., Prasanna Kumar, S., Bhattathiri, P.M.A., Kumar, M.D., Raghukumar, S., Nair, K.K.C., Ramaiah, N., 1996. Mechanism of the biological response to winter cooling in the north- eastern Arabian Sea. Nature (London) 384, 549–552.

Midhun Shah, H., Smitha, B.R., Mohamed Hatha, A.A., Sudhakar, M., 2019. Subsurface chlorophyll maxima in the North Eastern Arabian sea: Simulation on impact of warming. Ecol. Indic. 110 (2020), 105858.

Moran, X.A.G., Lopez-Urrutia, A., Calvo-Diaz, A., Li, W.K.W., 2010. Increasing importance of small phytoplankton in a warmer ocean. Glob. Chang. Biol. 16, 1137–1144.

Narasimha Rao, T.V., 2002. Spatial distribution of upwelling off the Central East Coast of India. Estuar. Coast. Shelf Sci. 54, 141–156.

Narvekar, Jayu, Joshua Rosario, D., Mello, S.Prasanna, Kumar, Prinyanka Banerjee, Sharma, Vrinda, Shenai-Tirodkar, Prachi, 2017. Winter-time variability of the estern Arabian Sea: a comparison between 2003 and 2013. Geophys. Res. Lett. 44. https://doi.org/10.1002/2017GL072965.

Okubo, A., 1970. Horizontal dispersion of floatable particles in the vicinity of velocity singularities such as convergences. Deep-Sea Res. Oceanogr. Abstr. 17, 445–454. https://doi.org/10.1016/0011-7471(70)90059-8.

Owens, N.J.P., Burkill, P.H., Mantoura, R.F.C., Woodward, E.M.S., Bellan, I.E., Aiken, J., Howland, R.J.M., Llewellyn, C.A., 1993. Size-fractionated primary production and nitrogen assimilation in the northwestern Indian Ocean. Deep-Sea Res. II Top. Stud. Oceanogr. 40 (3), 697–709.

Parsons, T.R., Maita, Y., Lalli, C.M., 1984. A Manual of Chemical and Biological Methods for Seawater Analysis. Pergamon00 Press, New York, p. 173 (1984).

Platt, T., Bird, D.F., Sathyendranath, S., 1991. Critical depth and marine primary production. Proc. R. Soc. B 246, 205–217.

Pond, S., Pickard, G.L., 1993. Introductory Dynamic Oceanography. Pergamon Press, New York 240pp.

Prasanna Kumar, S.P., Roshin, Raj P., Narvekar, Jayu, Kumar, P.K.Dinesh, Vivekanandan, E., 2009. Response of the Arabian Sea to global warming and associated regional climate shift. Mar. Environ. Res. 68, 217–222.

Rao, R.R., Kumar, M.S.Girish, Ravichandran, M., Rao, A.R., Gopalakrishna, V.V., Thadathil, P., 2010. Interannual variability of Kelvin wave propagation in the wave guides of the equatorial Indian Ocean, the coastal Bay of Bengal and the southeastern Arabian

Sea during 1993–2006. Deep-Sea Res. I Oceanogr. Res. Pap. 57 (1), 1–13 January 2010.
Roxy, M.K., Ritika, K., Terray, P., Masson, S., 2014. The curious case of Indian Ocean warming. J. Clim. 27 (22), 8501–8509.
Roxy, Mathew Koll, Modi, Aditi, Murtugudde, Raghu, Valsala, Vinu, Swapna Panickal, S., Prasanna Kumar, M., Ravichandran, Marcello Vichi, Lévy, Marina, 2016. A reduction in marine primary productivity driven by rapid warming over the tropical Indian Ocean. Geophys. Res. Lett. 43, 826–833. https://doi.org/10.1002/2015GL066979.
Sanjeevan, V.N., Smitha, B.R., Abdul Jaleel, K.U., Jayalalshmi, K.J., Ashadevi, C.R., 2011. Re-validation of Potential Yield from Indian EEZ.A trophodynamic approach. Report of the Working Group for Revalidating the Potential of Fishery Resources in the Indian EEZ. Ministry of Agriculture, New Delhi, pp. 50–60.
Shetye, S.R., Gouveia, A.D., Shenoi, S.S.C., 1994. Circulation and water masses of the Arabian Sea. Proc. Indian. Acad. Sci (Earth Planet. Sci.) 103 (2), 107–123.
Singh, A., Ramesh, R., Godhe, A., 2014. Inter- and intra-specific carbon and nitrogen assimilation by dinoflagellates and diatom species. Curr. Sci. 106 (6), 867–870.
Smitha, B.R., Rafeeq, M., Sanjeevan, V.N., Padmakumar, K.B., Thomas, Lathika C., Devi, C.R. Asha, Dwivedi, R.M., 2013. Short term eddies in the North Eastern Arabian Sea trigger high biological production during Spring Inter Monsoon. Proceedings of National Conference OSICON 2013 "Role of Oceans in Earth System", IITM, Pune, 26-28 November 2013, pp. 379–382.
Sriwoon, R., Pholpunthin, P., Lirdwitayaprasit, T., Kishino, M., Furuya, K., 2008. Population dynamics of green Noctiluca scintillans (Dinophyceae) associated with the monsoon cycle in the upper gulf of Thailand. J. Phycol. 44, 605–615.
Sushma, G. Parab, Matonkar, S.G. Prabhu, Raman, Mini, Dwivedi, R.M., 2012. Distribution and ecology of the Trichodesmium spp. in the Arabian Sea: ship and satellite studies. Proceedings 11th Biennale conference of Pan Ocean Remote Sensing Conference, 5-9 November 2012, Kochi, India.
Sverdrup, H.U., 1953. On conditions for the vernal blooming of phytoplankton. J. Cons. Int. Explor. Mer 18, 287–295.
Tada, K., Pithakpol, S., Montani, S., 2004. Seasonal variation in the abundance of Noctiluca scintillans in the Seto Island Sea, Japan. Plankton Biol. Ecol. 51, 7–14.
Tomas, C.R., 1997. Identifying Marine Phytoplankton. Acad. Press, San Diego, p. 858 (1997).
Toseland, Daines, A.S.J., Clark, J.R., Kirkham, A., Strauss, J., Uhlig, C., Lenton, T.M., Valentin, K., Pearson, G.A., Moulton, V., Mock, T., 2013. The impact of temperature on marine phytoplankton resource allocation and metabolism. Nat. Clim. Chang. https://doi.org/10.1038/NCLIMATE1989 8 SEPTEMBER 2013.
Turner, J.S., 1973. Buoyancy Effects in Fluids. Cambridge Univesity Press, p. 250.
Vidya, P.J., Siby, Kurian, 2018. Impact of 2015–2016 ENSO on the winter bloom and associated phytoplankton community shift in the northeastern Arabian Sea. J. Mar. Syst. 186 (2018), 96–104.
Weiss, J., 1991. The dynamics of enstrophy transfer in two-dimensional hydrodynamics. Physica D 48, 273–294. https://doi.org/10.1016/0167-2789(91)90088-q.
Wiggert, J.D., Jones, B.H., Dickey, T.D., Brink, K.H., Weller, R.A., Marra, J., Codispoti, L.A., 2000. The northeast Monsoon's impact on mixing, phytoplankton biomass and nutrient cycling in the Arabian Sea. Deep-Sea Res. II 47, 1353–1385.
Wiggert, J.D., Hood, R.R., Banse, K., Kindle, J.C., 2005. Monsoon-driven biogeochemical processes in the Arabian Sea. Prog. Oceanogr. 65 (2–4), 176–213.
Xiang, Chenhui, Tan, Yehui, Zhang, Huangchen, Ke, Jiaxing Liu Zhixin, Li, Gang, 2019. The key to dinoflagellate (Noctiluca scintillans) blooming and outcompeting diatoms in winter off Pakistan, northern Arabian Sea. Sci. Total Environ. 694 (2019), 133396.